Article

Serial clustering of intense European storms

RENATO VITOLO[1*], DAVID B. STEPHENSON[1], IAN M. COOK[2] and KIRSTEN MITCHELL-WALLACE[2]

[1]School of Engineering, Computing and Mathematics, University of Exeter, UK
[2]Willis Re, London, UK

Abstract

This study has investigated how the clustering of wintertime extra-tropical cyclones depends on the vorticity intensity of the cyclones, and the sampling time period over which cyclone transits are counted. Clustering is characterized by the dispersion (ratio of the variance and the mean) of the counts of eastward transits of cyclone tracks obtained by objective tracking of 850 hPa vorticity features in NCEP-NCAR reanalyses. The counts are aggregated over non-overlapping time periods lasting from 4 days up to 6 month long October-March winters over the period 1950–2003. Clustering is found to be largest in the exit region of the North Atlantic storm track (i.e. over NE Atlantic and NW Europe). Furthermore, it increases considerably for the intense cyclones, for example, the dispersion of the 3-monthly counts near Berlin increases from 1.45 for all cyclones to 1.80 for the 25 % most intense cyclones. The dispersion also increases quasi-linearly with the logarithm of the length of the aggregation period, for example, near Berlin the dispersion is 1.08, 1.33, and 1.45 for weekly, monthly, and 3-monthly totals, respectively. The increases and the sampling uncertainties in dispersion can be reproduced using a simple Poisson regression model with a time-varying rate that depends on large-scale teleconnection indices such as the North Atlantic Oscillation, the East Atlantic Pattern, the Scandinavian pattern, and the East Atlantic/West Russia pattern. Increased dispersion for intense cyclones is found to be due to the rate becoming more dependent on the indices for such cyclones, whereas increased dispersion for longer aggregation periods is related to the small amounts of intraseasonal persistence in the indices. Increased clustering with cyclone intensity and aggregation period has important implications for the accurate modelling of aggregate insurance losses.

Zusammenfassung

Die vorliegende Studie analysiert den Zusammenhang zwischen der seriellen Häufung von winterlichen extratropischen Zyklonen und der Wirbelstärkeintensität der Zyklonen sowie der Länge des Zeitintervalls, über das die Zyklonendurchgänge akkumuliert werden. Dabei wird die serielle Häufung charakterisiert durch die statistische Dispersion (dem Quotienten aus Varianz und Mittelwert) in der Anzahl der ostwärts ziehenden Zyklonen. Diese Anzahl kann durch objektive Verfolgung der Eigenschaften der 850 hPa-Wirbelstärke in NCEP-NCAR-Reanalysen ermittelt werden. Die Akkumulation der Anzahl erfolgt über disjunkte Zeitintervalle von minimal 4 Tagen bis maximal 6 Monaten (Oktober bis März) im Zeitraum von 1950 bis 2003. Die serielle Häufung ist am größten im Endgebiet des nordatlantischen Sturmkorridors (nordöstlicher Atlantik und nordwestliches Europa). Ausserdem kann ein erheblicher Zuwachs der seriellen Häufung bei stärkeren Zyklonen beobachtet werden; so wächst zum Beispiel die statistische Dispersion in der Anzahl der Zyklonen bei 3-Monats-Zeitintervallen von 1,45 für alle Zyklonen auf 1,80 für die 25 % stärksten Zyklonen an. Des weiteren wächst die statistische Dispersion etwa linear mit dem Logarithmus der Länge des Akkumulationszeitintervalls; nahe Berlin beträgt die statistische Dispersion zum Beispiel 1,08 für Wochen-, 1,33 für Monats-, und 1,45 für 3-Monats-Zeitintervalle. Sowohl die Zunahme als auch die Unsicherheit der statistischen Dispersion kann reproduziert werden mittels einfacher Poisson-Regressions-Modelle mit zeitabhängigen Raten, welche wiederum von großskaligen Telekonnektionsindizes (Nordatlantische Oszillation, Ostatlantisches Muster, Skandinavisches Muster und Ostatlantisches/Westrussisches Muster) abhängen. Die zunehmende statistische Dispersion bei starken Zyklonen kann durch die zunehmende Abhängigkeit dieser Raten von den Telekonnektionsindizes erklärt werden, wohingegen die zunehmende statistische Dispersion bei zunehmender Länge des Akkumulationszeitintervalls durch die langreichweitige serielle Korrelation der Telekonnektionsindizes erklärt wird. Zunehmende serielle Häufung bei zunehmender Zyklonenstärke und Länge des Akkumulationszeitintervalls spielt eine wichtige Rolle bei der zuverlässigen Modellierung von akkumulierten Versicherungsschäden.

1 Introduction

Intense extratropical cyclones are a major cause of insured loss in Europe. A recent example is windstorm *Kyrill*[1], which on 18th January 2007 affected the United Kingdom, Germany, the Netherlands, Belgium, Austria, the Czech Republic and Poland. An insured loss of €1 B (1.000 millions) for residential business was estimated by the German Insurance Association (GDV). Estimates for the overall insured market for this single event vary between €3.5 B (Swiss Re) and €5-7 B (Munich Re, Hannover Re), see WILLIS ANALYTICS (2007).

Clusters of intense windstorms are particularly threatening. A cluster is a group of windstorms occurring in

---

*Corresponding author: Renato Vitolo, School of Engineering, Computing and Mathematics, University of Exeter, Harrison building, North Park Road, EX4 4QF, UK, e-mail: r.vitolo@exeter.ac.uk
[1]http://www.met.fu-berlin.de/wetterpate

a short time span: this may affect either the same geographical region or, from an insurer viewpoint, the same portfolio of insured properties. An example is provided by the December 1999 windstorms *Anatol*, *Lothar* and *Martin*, which caused a total in excess of $15 B of damage, of which nearly $11 B insured (MAILIER, 2007). Given the typical structure of non-proportional reinsurance contracts, the net impact of a series of losses to an insurance company depends not only on the total loss but also on the number of distinct loss events. A cluster of events can cost an insurance company (after reinsurance) much more than a single event with the same total loss (before reinsurance). The reinsurance industry uses computer catastrophe (CAT) models to estimate potential losses for a portfolio of policies. CAT models traditionally assumed[2] that catastrophic events occur independently of each other at a constant *rate* (average event frequency in time). These assumptions lead to underestimation of temporal clustering and related risk. Another factor for insurers is that regulatory capital requirements are increasingly moving towards being set as a high percentile (e.g. 99.5 %) of the modelled distributon of total losses. Clustering of ETCs can have an important impact on this distribution at such percentiles.

Temporal clustering of extratropical cyclones has recently been noted in the scientific literature by MAILIER et al. (2006); MAILIER (2007). They examined Oct-Mar winter cyclone tracks in the NCEP-NCAR reanalysis and found two large regions with significant clustering: in the central North Pacific and near the exit of the North Atlantic storm track. KVAMSTØ et al. (2008) found that cyclone clustering is substantially underestimated by the ARPEGE general circulation model near the storm track exit region. In these studies, clustering is measured by a dispersion statistic defined as the ratio of variance to mean of monthly counts of cyclones crossing 'barriers' along meridians (or parallels). The main mechanism proposed to explain the overdispersion is the time-varying effect of the large-scale flow on the individual cyclone tracks.

The present work is motivated by the following more detailed questions:

1. How does clustering behave for more intense cyclones (rather than all cyclones)?

2. How does clustering depend on the period over which the cyclone transits are aggregated?

3. How does clustering depend on the width of the 'barriers'?

---

[2]A recent upgrade of RMS Simulation Platform (www.rms.com/) incorporates clustering of weather events. Also see www.air-worldwide.com/_public/html/air_currentsitem.asp?ID=1425 for AIR research on the subject.
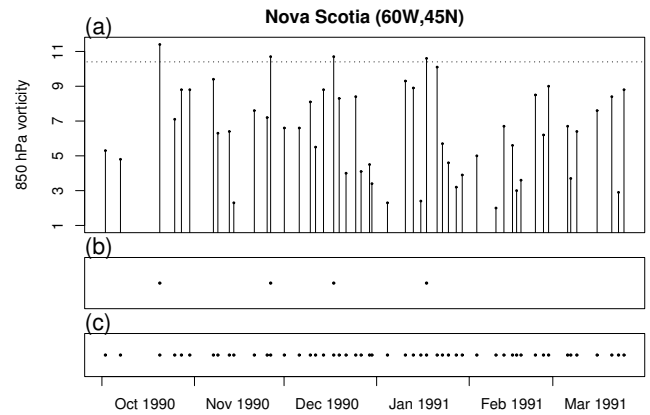
Figure 1: Portion of time series of cyclone transits (c) and associated vorticities (a) at a gridpoint near Nova Scotia (60°W,45°N), during extended winter October 1990-March 1991. A horizontal dotted line in (a) marks the 90 % quantile of the vorticity distribution at that gridpoint (value is $10.4 \times 10^{-5} s^{-1}$), corresponding transits are marked in (b).
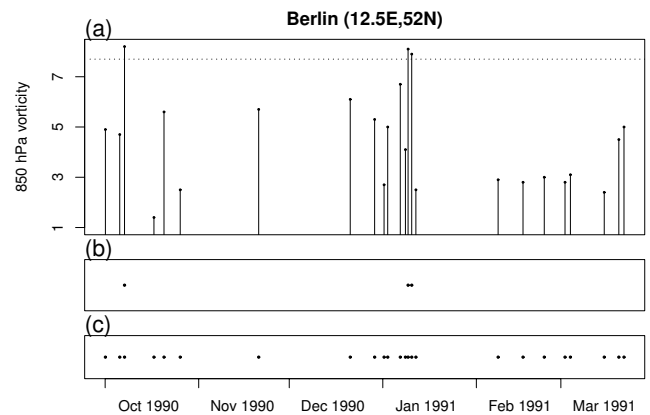

Figure 2: Same as Fig. 1 for a gridpoint near Berlin (12.5°E,52°N). The 90 % vorticity quantile is here $7.7 \times 10^{-5} s^{-1}$.

The results presented here indicate that in the northeastern Atlantic and in northwestern Europe the clustering increases considerably for more intense cyclones and with the barrier width. Also clustering increases with the length of aggregation period in a spatially coherent way. The time-varying effect of four teleconnection indices (for the North Atlantic Oscillation, east Atlantic pattern, Scandinavian pattern, east Atlantic-western Russian pattern) accounts for the above behaviour to a large extent.

2 The extratropical cyclone database

The same database of Northern Hemisphere cyclone tracks as in MAILIER et al. (2006) is used here. This covers 53 extended winters (October-March), from Oct 1950 to Mar 2003 and is obtained from the NCEP/NCAR reanalysis dataset (KALNAY et al., 1996). Cyclone centres are identified as maxima of the relative vorticity ξ_{850} of the wind field at 850-mb. The tracking
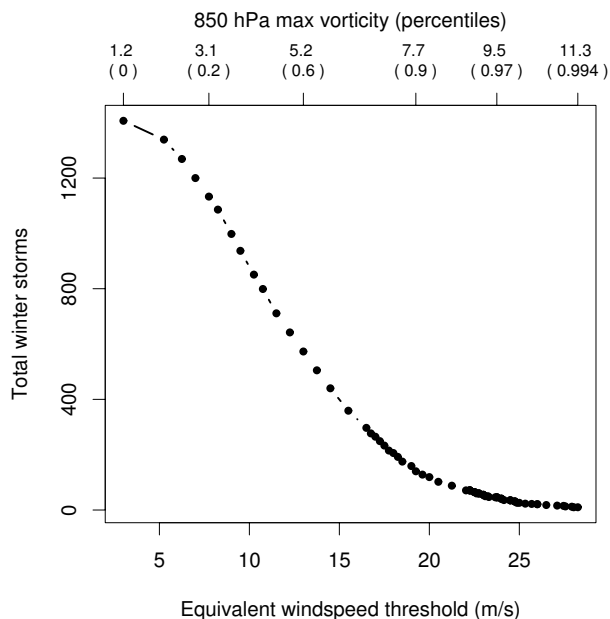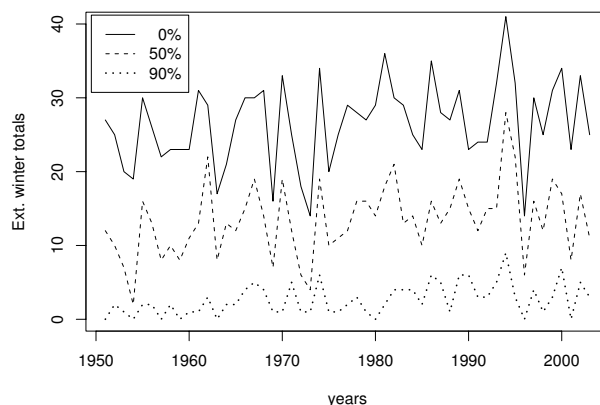
Figure 3: Total number of extended winter cyclone transits through a gridpoint near Berlin (12.5°E,52°N) as a function of the vorticity threshold used to select the intense cyclones. Thresholds of relative vorticity at 850 hPa and corresponding quantiles are given in the top horizontal axis, whereas the bottom axis reports windspeeds at $r = 500$ km distance from the centre, according to (2.1).


Figure 4: Time series of extended winter totals of cyclone transits through the approximate location of Berlin (12.5°E,52°N), for three different values of the 850 hPa relative vorticity threshold $\bar{\xi}_{850}$ used to select the intense cyclones: $\bar{\xi}_{850} = 1.2 \times 10^{-5} s^{-1}, 4.6 \times 10^{-5} s^{-1}$ and $7.7 \times 10^{-5} s^{-1}$, corresponding to 0 %, 50 % and 90 % quantiles of the vorticity distribution at that gridpoint.

of the cyclones across consecutive 6-hourly timesteps is performed by Hodges' algorithm (HODGES, 1994, 1995, 1996, 1999). We refer to MAILIER (2007, Chapter 3) for details.

Given the focus on western Europe, the domain considered here is (125°W,45°E) in longitude and (20°N,80°N) in latitude. For each point on a grid with spacing 2.5°, a time series of cyclone transits is constructed in the same way as MAILIER et al. (2006): eastward cyclone transits across the local meridian within ±10° of latitude from the gridpoint are first identified. For each cyclone, only the first eastward transit is retained, to exclude the occurrence of multiple counts arising from the same recurring cyclone. Indeed, due to the definition of "events" in reinsurance contracts, recurring storms are not identified as distinct events. Moreover, multiple counts due to recurring cyclones are rare MAILIER et al. (2006). The time and relative vorticity of each transit are computed by linear interpolation between the nearest points along the cyclone trajectory on each side of the crossed meridian. Examples are given in Figs. 1 and 2, for gridpoints near Nova Scotia and Berlin, respectively. Cyclone transits can occur in a regular fashion (Fig. 1) or in clusters (Fig. 2).

Our main aim is to quantify the dependence of such clustering on cyclone intensity, with a rough measure of intensity provided by the relative vorticity ξ_{850}. For a fixed gridpoint, an *intensity threshold* is chosen as a quantile of the distribution of ξ_{850} for all cyclone transits at that gridpoint. The transit time series is then

"thinned" by selecting cyclones whose vorticity exceeds the threshold. This is illustrated in Fig. 2, where a dotted line represents the threshold $\bar{\xi}_{850} = 7.7 \times 10^{-5} s^{-1}$, corresponding to the 90 % quantile of the vorticity distribution at that gridpoint. The above procedure is repeated for the same gridpoint near Berlin as in Fig. 2, for values of the vorticity threshold $\bar{\xi}_{850}$ ranging from 0 % to 99.4 %. The corresponding relative vorticity distribution is shown in Fig. 3. Values of $\bar{\xi}_{850}$ are plotted in the top horizontal axis (corresponding quantiles in parentheses). The number of cyclones whose vorticity exceeds the threshold specified on the horizontal axis is plotted in the vertical axis. A coarse measure u of equivalent windspeed is derived by considering the cyclone as a rotating solid disk of air with radius r in the 850 mb geopotential surface: an application of Stokes' theorem (see (MAILIER, 2007, Sec. 4.5.3.4)) gives

$$2\pi u = \pi r^2 \xi_{850}, \qquad (2.1)$$

from which u can be derived as a function of ξ_{850}. The bottom horizontal axis of Fig. 3 displays windspeeds $\bar{u}$ equivalent to vorticity thresholds $\bar{\xi}_{850}$ (top horizontal axis) through (2.1) with $r = 500$ km. Note that this measure of windspeed strongly underestimates the observed peak gust velocities: for example, the maximum equivalent windspeed for the December 1999 freak storms Lothar and Martin is $u = 26$ and 16 ms^{-1}, respectively, against observed peak gust velocities of $u = 50$ and 48 ms^{-1}, respectively (BRESCH et al., 2000).

The time series of transits as in Fig. 1 are turned into time series of transit counts by fixing an aggregation period Δt and counting all transits occurring within consecutive time intervals of width Δt: this is a sort of "binning in the time axis" for the all 53 extended winters.
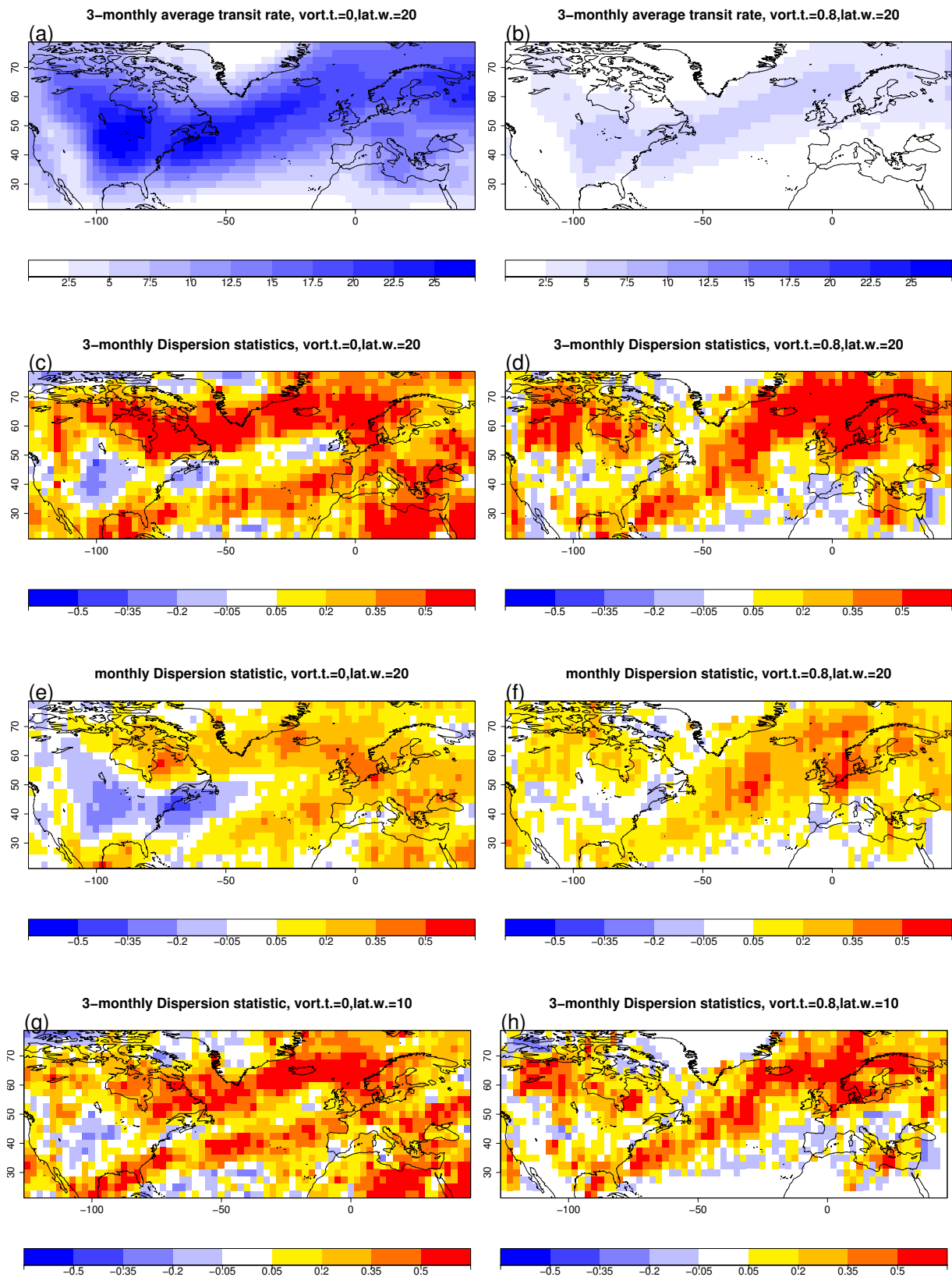
Figure 5: (a) Average cyclone transit rate at each gridpoint, using the whole cyclone database and a 3-monthly aggregation period. (b) same as (a), where for each gridpoint only the cyclones exceeding the 80 % quantile of the vorticity distribution at that gridpoint are retained ("v.t." stands for vorticity threshold, "lat.w." for latitudinal width of the barrier). (c),(d) dispersion statistic of the cyclone count series of (a) and (b), respectively. (e),(f) same as (c),(d) with an aggregation period of 1 month. (g),(h) same as (c),(d) with a barrier of 10° latitudinal witdh.

Notice that Δt was fixed to 1 month in MAILIER et al. (2006): both shorter periods (such as 2, 7 and 14 days) and longer periods (2 and 3 months, as well as the whole extended winter from 1 October to 31 March, which is 182 days long in non-leap years) are considered here. This is illustrated for the same gridpoint near Berlin as in Fig. 2: the time series of the transit counts in each extended winter in the database (that is for $\Delta t = 182$) is shown in Fig. 4, for three values of the relative vorticity threshold ξ_{850}. Strong interannual variations occur for each threshold value and a slight increasing trend is visible.

3 Dispersion of counts: a measure of clustering

The occurrence of pointwise events in the time axis, such as those in Fig. 1, can be modelled by a Poisson stochastic process (COX and ISHAM, 1980). A simple homogeneous Poisson process (SHPP) is a collection $\{N_t, t \geq 0\}$ of random variables, where N_t is the number of events that have occurred up to time t, starting from 0 and satisfying certain properties (see e.g. MAILIER et al. (2006, Appendix)): among them, the *memorylessness* implies that the number of arrivals in any bounded interval after time t is independent of the number of arrivals occurring before time t. Therefore, this independence assumption amounts to *complete serial randomness* in time.

The procedure of aggregating cyclone transits into sequences of transit counts (see previous section) leads to consider the Poisson distribution: an integer-valued random variable Y is Poisson distributed when the probability of observing a count of $k \geq 0$ is equal to

$$P[Y = k] = e^{-\mu}\mu^k/k! \qquad (3.1)$$

for some $\mu > 0$. In loose words, the Poisson distribution is obtained from the Poisson process by "binning" in the time axis, as described in the previous section. More precisely, if the average rate of arrival in a SHPP is $\lambda > 0$, then the number $N_{t_1} - N_{t_0}$ of arrivals during the time interval $\Delta t = t_1 - t_0$ is Poisson distributed with mean $\mu = \lambda \Delta t$.

The Poisson distribution is characterised by equality of mean and variance (equidispersion): $\mathbb{V}ar(Y) = \mathbb{E}(Y) = \mu$. This is a fairly strong restriction: observed count data are seldom equidispersed (CAMERON and TRIVEDI, 1998). Overdispersion ($\mathbb{V}ar(Y) > \mathbb{E}(Y)$) is often found, whereas underdispersion ($\mathbb{V}ar(Y) < \mathbb{E}(Y)$) is less common. Following the approach by MAILIER et al. (2006), a sample dispersion statistic ψ is introduced:

$$\psi = \mathbb{V}ar(Y)/\mathbb{E}(Y) - 1. \qquad (3.2)$$

Clustering of cyclone transits is characterised by the dispersion statistic (3.2), which quantifies deviation from equidispersion (Poissonianity) of the distribution of

transit counts. Clustering is of relevance to the insurance industry due to the typical structure of non-proportional reinsurance contracts and the capital requirements discussed in the Introduction. For example, assume that an insurance company buys reinsurance covering 2 events per year, with an exceedance probability level of 15 %. If events are Poisson distributed ($\psi = 0$) then the probability p_3 of having more than two events per year is 0.1 %. However, if events are distributed according to a negative binomial (CAMERON and TRIVEDI, 1998) with $\psi = 0.5$, then $p_3 = 0.8$ %, corresponding to an eightfold increase of the probability of a non-risk-managed situation.

In MAILIER et al. (2006) it has been shown that large regions in the Northern Hemisphere are characterised by overdispersion of the cyclone transit counts: the gridpoint of Fig. 2 falls in this class. Underdispersion is also found, although it is confined to regions of strong baroclinic development. The gridpoint in Fig. 1 is contained in one of these regions.

## 4 Dependence of dispersion on cyclone intensity and aggregation period

The three questions at the end of the Introduction are now dealt with. It is shown that overdispersion is larger for the more intense cyclones in Northern Europe near the exit of the storm track is larger. Overdispersion also increases for larger values of Δt and decreases for narrower latidudinal barriers. The variation of dispersion with cyclone intensity has a more regional character.

For each gridpoint cyclone transit are aggregated over a period of 3 months (see Sec. 2), that is for each Oct-Nov-Dec and Jan-Feb-March period, yielding series of length 106. Fig. 5 (a) show the average transit rate at each gridpoint, defined as the ratio between the total number of transits and the total length of the time series. Fig. 5 (b) shows the transit rate of cyclones whose vorticity exceeds the 80 % quantile of the vorticity distribution at that gridpoint. For shortness, these will be referred to as "intense cyclones" throughout the rest of the paper. This definition is purely empirical: it has been chosen as a compromise between having as high threshold as possible, while still retaining a number of cyclones which is sufficient for statistical analysis.

The region near the entrance of the North Atlantic storm track is characterised by underdispersion, whereas overdispersion is found near the exit of the storm track (centre and bottom rows of Fig. 5). This holds both for the monthly and the 3-monthly aggregation period and was already observed in MAILIER et al. (2006) for the monthly period. An increase of dispersion with intensity is observed in the 3-monthly counts for intense cyclones near the end of the storm track: compare Fig. 5 (c) and (d). This region includes a part of Europe around the North Sea, comprising the eastern side of the British Isles, a large part of the Scandinavian peninsula and Denmark. The southern edge of this region includes

850 hPa vorticity percentiles (storm numbers)
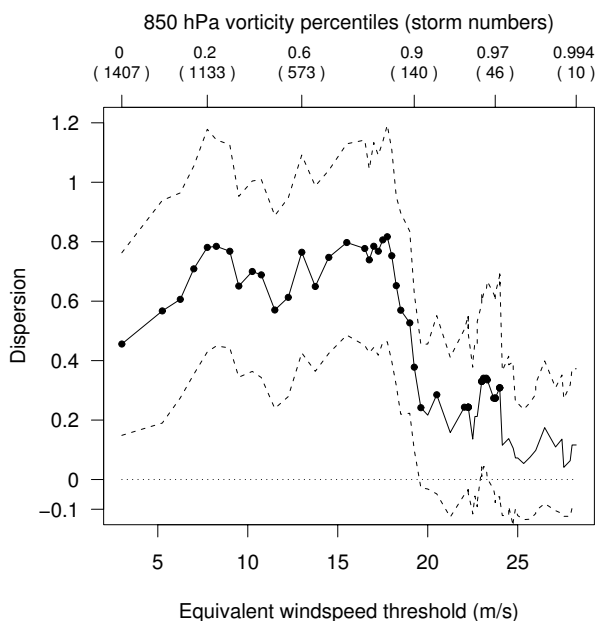
Berlin (12.5,52)

Figure 6: Dispersion statistic (solid line) and 90 % bootstrap confidence interval (dashed) of the 3-monthly cyclone counts at the approximate location of Berlin (12.5°E,52°N) as a function of the 850 hPa relative vorticity threshold used to select the most intense cyclones. Thick dots: values of ϕ which are significant according to a Katz test at the 10 % confidence level (see Appendix). The relation between vorticity and equivalent windspeeds is (2.1), compare Fig. 3.
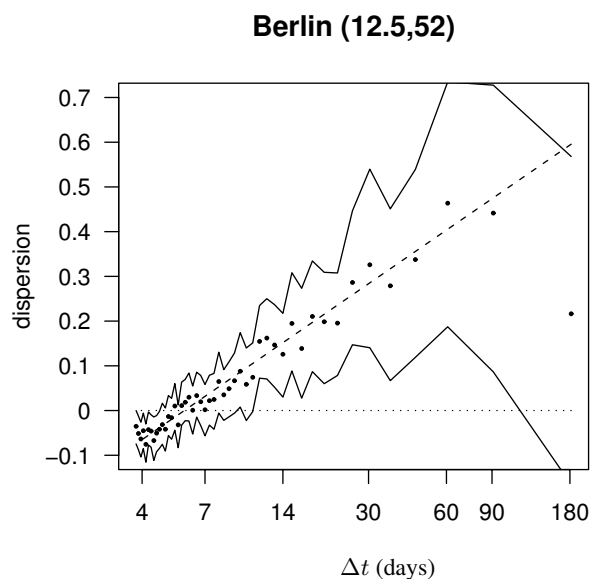
Figure 7: Dispersion statistic ψ (points) of the cyclone transit counts versus aggregation period Δt, at the approximate location of Berlin (12.5E,52N). Logarithmic scale is used in the horizontal axis. 90 % confidence intervals (solid lines) are computed as quantiles of a bootstrap sample for each Δt. A linear regression fit of ψ versus $\log(\Delta t)$ is added (dashed line; the point with $\Delta t = 182$ was not included in the regression).

part of Northern Germany and France, as well as the Benelux countries. In this same region, overdispersion also increases when passing from the monthly to the 3-monthly aggregation period, compare panels (c) (d) to panels (e) (f), respectively, in Fig. 5. This is observed for both the whole cyclone dataset (panels (c) (e)) and when restricting to the intense cyclones (panels (d) (f)). Raising the vorticity threshold induces a decrease in dispersion in North East Canada and part of Southern Europe including Spain and Italy, both for the monthly and 3-monthly aggregation periods (Fig. 5 (c)–(d)).

A general increase of dispersion with aggregation period is observed: the spatial coherence of this phenomenon is larger than that of the increase of dispersion with cyclone intensity, which has a more regional character (see above). The dispersion increases for larger aggregation periods in nearly the whole selected domain: compare Fig. 5 (c) and (e) (where all cyclones are taken into account). The increase is more pronounced at the sides of the North Atlantic storm track, particularly so in a large region comprising North East Canada, Iceland and bordering the Scandinavian peninsula and in nearly all gridpoints in continental Europe. Lastly, the dispersion decreases for narrower latitudinal barriers (panels (g) (h)), although it remains large around the North Sea also for the intense cyclones.

Fig. 6 shows the dispersion statistic ψ as a function of the vorticity threshold $\bar{\xi}_{850}$, for the same gridpoint as

Fig. 3. Notice that a different transit count time series is constructed for each threshold value. The dispersion initially increases with the threshold, then remains roughly constant up to vorticity quantiles of about 80 %. The point estimates of the dispersion range from 0.4 to nearly 0.8: these are very large values from the point of view of risk management. At the 90 % quantile the dispersion is 0.38. For quantiles between 0.9 and 0.97 ψ varies between 0.2 and 0.34 (most of these values are significant according to a Katz test at the 10% confidence level, see Appendix); ψ and it drops down to about 0.2 for larger quantiles. Uncertainties are here extremely large: for a threshold $\bar{\xi}_{850}$ of 85 %, the confidence interval of ψ ranges, approximately, from 0.4 to 1.17. This large amount of uncertainty poses serious problems from the point of view of risk management. Confidence intervals are computed by bootstrap (DAVISON and HINKLEY, 1997): for each threshold value, a sample of 400 replicates is generated from the the corresponding count series and the 5 % and 95 % empirical quantiles of this sample define a 90 % confidence interval (dashed lines in Fig. 6). This is in fact block-bootstrap, since the aggregate counts in each period are shuffled, not the individual cyclone occurrences.

Fig. 7 shows a plot of ψ as a function of Δt for the same gridpoint as above (using all cyclones). The underdispersion occurring at the smaller periods (3/4 days) is due to inhibition (see MAILIER (2007, Sec. 4.5.3.3)):

Berlin (12.5E,52N): all storms
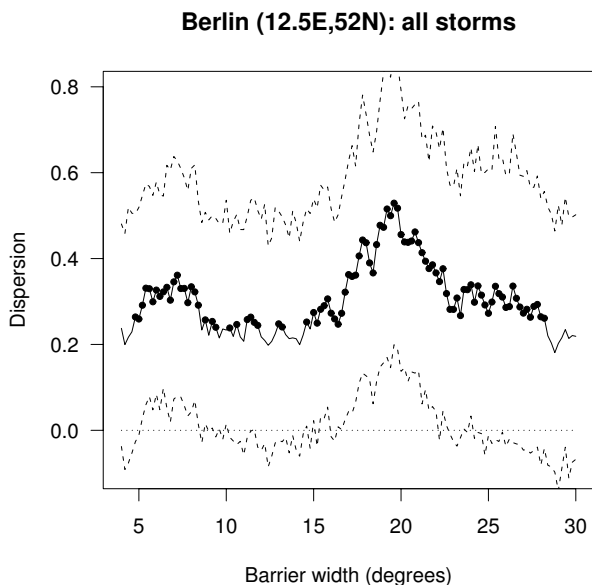
Figure 8: Dispersion statistic ψ (solid line) for all cyclones and 90 % confidence interval (dashed) versus width of the latitudinal barrier used to define the cyclone transits (same gridpoint as Fig. 7). Thick dots: values of ϕ which significant according to a Katz test at the 10 % confidence level (see Appendix).

Berlin (12.5E,52N): vort.t. 0.9
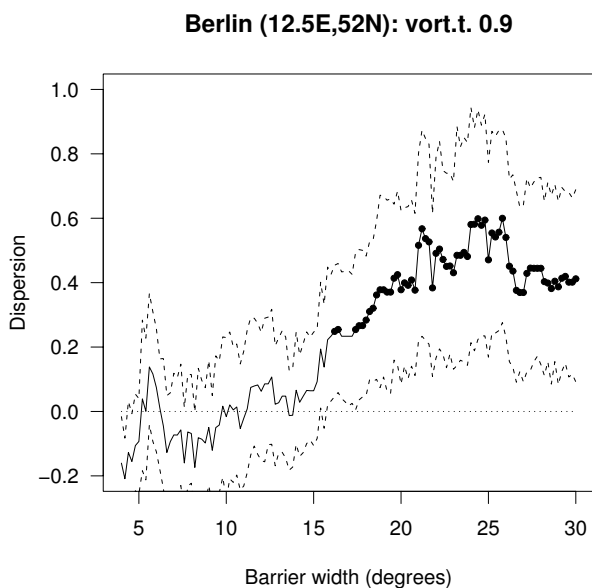
Figure 9: Same as Fig. 8 for the cyclones whose vorticity exceeds a threshold of 90 % of the vorticity distribution.

consecutive cyclone transits cannot occur indefinitely close to each other due to the spatial extension of the extratropical cyclones (typically, 1,000–2,000 km in diameter). Correspondingly, the lag-1 and lag-2 autocorrelations of the transit counts for the shorter aggregation periods are significantly different from zero (not shown).

For larger aggregation periods, e.g. 14 days, the lag-2 autocorrelation is not significantly different from zero at the 5 % confidence level (whereas the lag-1 autocorrelation is).

A linear scaling of the form $\psi = a \log(\Delta t) + b$ is obeyed to a good approximation for Δt ranging from a few days up to three months. A linear fit of ψ versus $\log(\Delta t)$ is superimposed to Fig. 7: for this fit, only values of Δt up to 90 days have been used. In other words, the value of ψ obtained for $\Delta t = 182$ (corresponding to the whole extended winter) is treated as an outlier and removed from the dataset. Robust linear regression with M-estimators (VENABLES and RIPLEY, 1994), performed including this value as well, gives a comparable result. Uncertainty is very large for $\Delta t = 182$: the confidence interval ranges from below –10 % to nearly 60 % in Fig. 7. The corresponding sample is small: it consists of only 53 datapoints. Care should always be observed when finding indications of a scaling law: a rule of thumb (RUELLE, 1990) prescribes that a scaling should hold for at least three orders of magnitude and this is not true in our case. The features illustrated in Figs. 6 and 7 have been observed in several other locations, including gridpoints near Paris, Copenhagen, London. The increase of clustering with aggregation period, as well as the drop for the whole extended winter, occurs coherently in many locations (see Fig. 5).

Fig. 8 shows the dependence of ψ on the width of the latitudinal barrier used to define the cyclone transits. The overdispersion is nearly always statistically significant according to a Katz test at the 10 %, although uncertainty is very large. Fig. 9 shows that cyclone transits with vorticities above the 90 % threshold are generally underdispersed for widths up to 10 degrees whereas they are overdispersed for widths larger than 15 degrees approximately. Arguably the upper 90 % of the vorticity distribution identifies (damaging) windstorms. Fig. 9 suggests that windstorms exhibit serial clustering only on sufficiently wide spatial extensions. Therefore, windstorm clustering seems to be of concern for companies (such as reinsurance or large insurance groups) with spatially extended insurance portfolios. However, insurers with a more spatially localised portfolio might be affected by the accumulation of risk due to clustering of lower intensity storms ($\bar{\xi}_{850} = 80\%$,) indicated by Fig. 5 (d),(h). This is also relevant in view of the capital requirements discussed in the Introduction.

5 Can large-scale flow variations account for cyclone clustering?

In MAILIER et al. (2006) it has been shown that the time-varying effect of the large-scale atmospheric flow largely accounts for overdispersion in the monthly cyclone counts. Does the large-scale flow explain the increase of clustering with cyclone intensity displayed in Fig. 6? Does it explain the increase with aggregation period Δt, displayed in Fig. 7? The results of the present
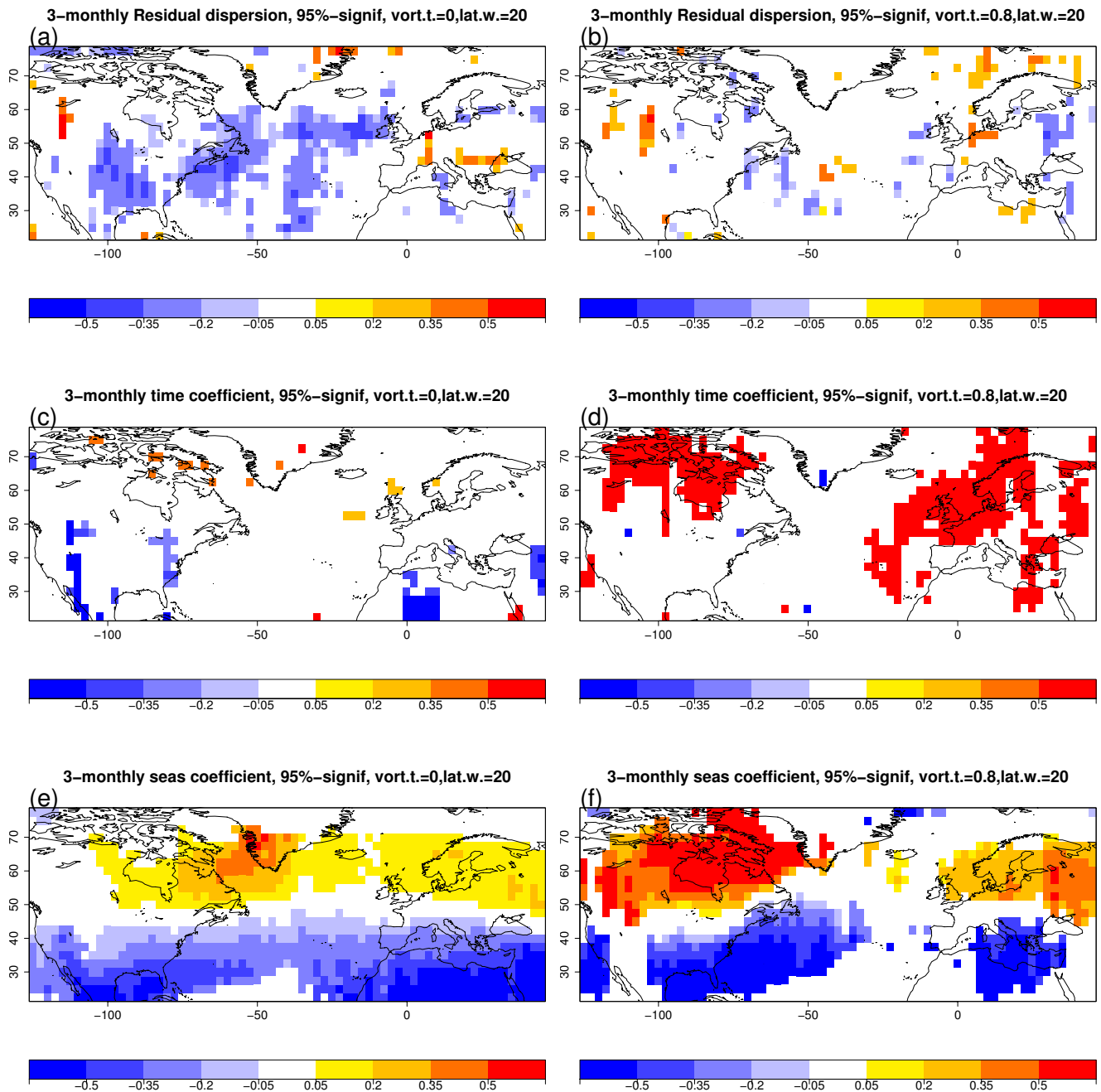
Figure 10: Residual dispersion of the Poisson regressions for each gridpoint, for the whole cyclone dataset (a) and for cyclones with vorticity above the 80 % quantile of vorticity distribution at that gridpoint (b). (c),(d) coefficient β_6 of the time trend in the Poisson regression, see Equation (5.2). (e),(f) same as (c),(d) for the coefficient β_5 of the seasonality. Only values significantly different from zero (according to a t-test at the 5 % confidence level) have been plotted.

section indicate so, across a range of cyclone intensities and aggregation periods.

A stochastic model as in MAILIER et al. (2006) constructed by Poisson regression (see the Appendix) is used to analyse the effect of the large-scale atmospheric flow on the cyclone transit count. In this study, we use daily values of the teleconnection indices for the the Northern Hemisphere, kindly provided by the Cli-

mate Prediction Center[3]. Rotated Principal Component Analysis (BARNSTON and LIVEZEY, 1987) is applied to monthly mean 700-mb geopotential height anomalies between January 1964 and July 1994. For every month of the year the 10 leading empirical orthogonal functions (EOFs) are selected and the amplitudes are standardised
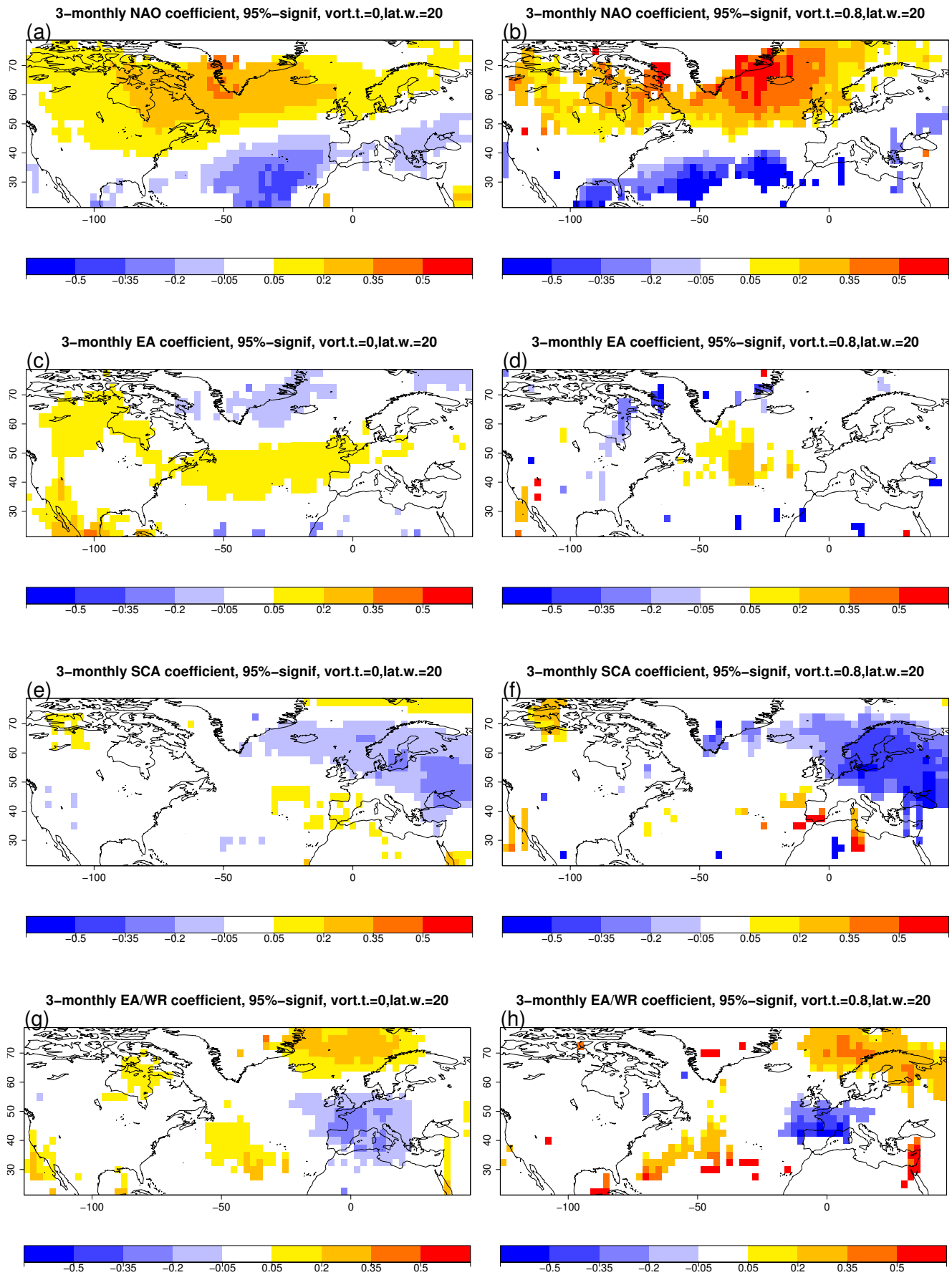
---

[3]http://www.cpc.ncep.noaa.gov/data/teledoc/telecontents.shtml

Figure 11: Same as Fig. 10 (c),(d) for the coefficients $\beta_1, \ldots, \beta_4$ of the teleconnection indices in (5.2) (from top to bottom).

to zero mean and unit variance. These indices are mutually uncorrelated by construction, which makes them particularly suitable for use as explanatory variables in the Poisson regression. Given the results of MAILIER et al. (2006) and after further testing, only the following indices have been retained: North Atlantic Oscillation (NAO), East Atlantic pattern (EA), Scandinavian Pattern (SCA) and East Atlantic/West Russia pattern (EA/WR). Terms accounting for season and for linear time trend have been included. For the 3-monthly count time series $Y = \{Y_j, j = 1, \ldots, n_Y\}$, we use the following Poisson Generalised Linear Model with log-link (see Apendix for explanation):

$$Y | X_1, X_2, \ldots, X_k \sim \text{Poisson}(\mu), \qquad (5.1)$$

$$\log(\mu) = \beta_0 + \sum_{i=1}^{k} \beta_i X_i, \qquad (5.2)$$

with $k = 6$, where $X_1, \ldots, X_4$ are the above teleconnection indices, X_5 is an indicator for the season (equal to 1 in October-December and 0 in January-March) and X_6 is a term expressing the logarithm of time j (suitably normalised between 0 and 1).

The Poisson model (5.1)-(5.2) captures the overdispersion in the cyclone transit counts, both for all cyclones and for the most intense ones: residual overdispersion is statistically significant, according to a Katz test at the 10 % level (see the Appendix), only in a few locations, see Fig. 10 (top row). One of these is a small area in Northern Germany: this is at the southern boundary of the region with strong overdispersion, surrounding the North Sea, described in the previous section. Coherently with MAILIER et al. (2006), residual underdispersion is found in a broad area within the North Atlantic, roughly centred around the locations where underdispersion occurs in the data, compare with Fig. 5, middle panel. However, much less residual underdispersion is found for the intense cyclones.

Pronounced non-stationarity is found for the intense cyclones. The linear trend coefficient β_6 is plotted in Fig. 10 (c),(d): for the intense cyclones β_6 is markedly positive over a large part of Northern Europe, including the Scandinavian peninsula, the British Isles, and Northern France and Germany (only values which are significant according to a t-test at the 5 % level have been plotted). Fig. 10 (d) suggests considerable upward trend in the average rate of intense cyclone transits: this is a potential indication of climatic change which is of particular relevance for the insurance industry and the society in general. However, the reader is warned that this might be an artifact of the inhomogenities which are found in reanalysis data (STERL, 2004). For example, such inhomogenities are the reason proposed by A. SMITS (2005) for the discrepancy in *sign* between the trends in storminess observed in station and in reanalysis data for the Netherlands. Seasonal variability also has very large effects on the cyclone transit rates (Fig. 10 (e),(f)): positive effects of the Oct-Dec indicator X_5 (see (5.1)-(5.2)) are

found throughout Northern Europe, whereas the subropical region is characterised by strong negative effects.

The variation of clustering with cyclone intensity shows a clear link with the large-scale atmospheric flow: the coefficients of the four teleconnection indices NAO, EA, SCA, EA/WR are significantly different from zero over large areas in the domain, see Fig. 11. In many cases it is found that the absolute value of the coefficients increases with the vorticity threshold (coefficients are plotted only if they are significant at the 5 % confidence level according to a t-test). An important issue in regression is selecting an appropriate subset of covariates from an initial set. The main criterion adopted here is according to whether the covariates contribute to explain clustering (overdispersion) in the count data (alternative approaches exist, such as Akaike's information criterion, or significance based on Wald or t-tests). Inclusion of the Polar-Eurasian (POL) index (which was used in MAILIER et al. (2006)) does not significantly improve the Poisson model fit over Europe: indeed the Poisson model in (5.1)–(5.2) performs well, as indicated by the residual dispersion plot in Fig. 10. Exclusion of any of the other four teleconnection indices yields deterioration of the model performance in capturing the overdispersion.

The effect of the large-scale flow on cyclone clustering is analysed in Fig. 12 for the same gridpoint as in Fig. 7, for several values of the vorticity threshold $\bar{\xi}_{850}$: for each of these, Poisson regression as in (5.1)-(5.2) is carried out on the corresponding sequence of cyclone transit counts. The dispersion predicted by the Poisson model is separately computed for each threshold by a parametric bootstrap approach; this method also gives estimates for the uncertainty in the dispersion, see the Appendix for details. The Poisson model captures several features of the behaviour in Fig. 6: the confidence intervals of the dispersion have roughly the same amplitude as for the data, see Fig. 12. The point estimate of the dispersion initially increases with the threshold, followed by a gradual decrease for the intense cyclones. The point estimates of dispersion for the data are nearly wholly contained in the 90 % confidence intervals of the Poisson-simulated dispersion and vice versa. However, the Poisson model does not fully capture the dispersion present in the data for thresholds between 20 % and 70 %: the discrepancy in the point estimates is fairly large there (up to 0.3). This is not an effect of seasonal dependence or long-term trend alone, although both are present (see Fig. 10 (d)). Removing the trend term from the covariates has little effect, whereas removing the seasonal term slightly reduces the amount of modelled overdispersion (not shown). Therefore, these terms alone do not explain the overdispersion in the observed data.

Monthly aggregation periods are used in Fig. 13. The shape of the dispersion as a function of the threshold $\bar{\xi}_{850}$ is similar to Fig. 12: an initial increase is followed by a decrease for large thresholds. However, the confidence intervals are smaller for the monthly counts. A Poisson regression model is set-up for the monthly
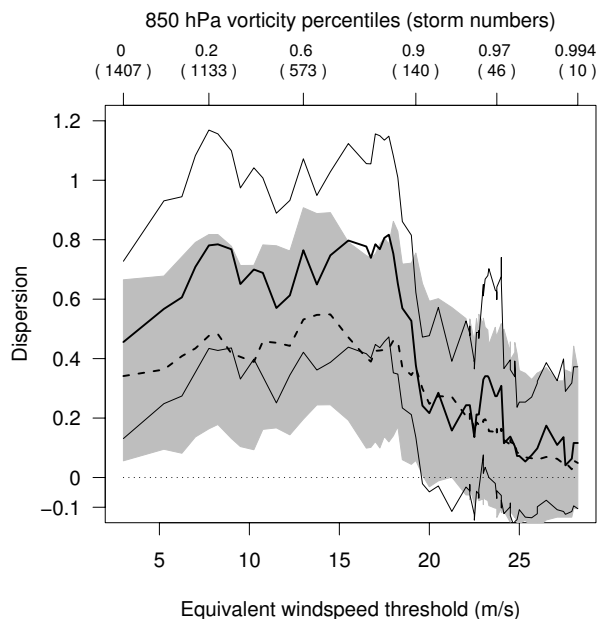
Figure 12: Same as Fig. 6 (solid lines), where the dispersion simulated by the Poisson regression model is added (dashed line) and its 90 % bootstrap confidence intervals for each threshold value are rendered with grey shading.
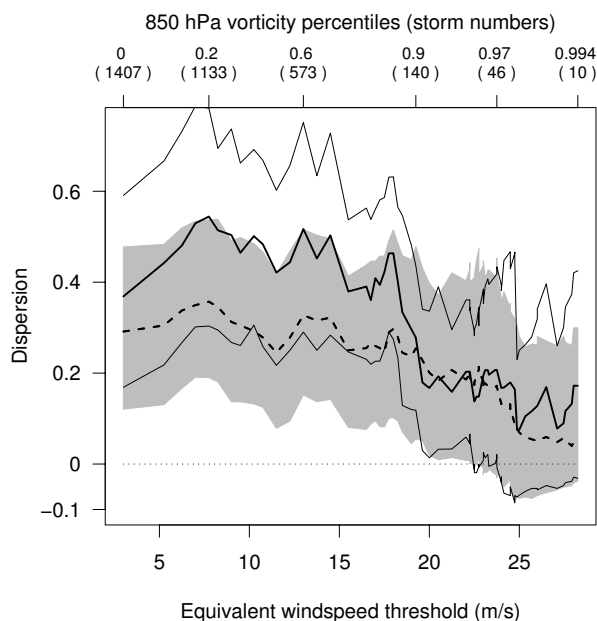
**Figure 13:** Same as Fig. 12 for the monthly cyclone counts.

counts as in MAILIER et al. (2006): five seasonal indicators are used for the months October-February (instead of the single term X_5 used for the 3-monthly counts). This model captures the dispersion in the monthly counts in a reasonable way: Poisson-based confidence intervals include nearly all the point estimates for the data and viceversa. Also, the width of the Poisson-based confidence intervals is comparable to that of the data.
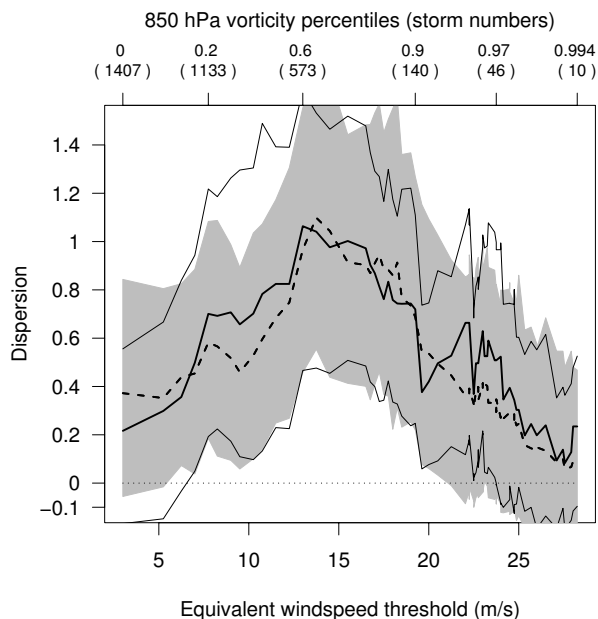

Figure 14: Same as Fig. 13 for the yearly cyclone counts.

In this case as well (compare the above discussion for Fig. 12), linear time trend does not account for the overdispersion, since its removal from the covariates reduces the amount of modelled dispersion by only a slight amount (not shown). On the other hand, removal of the indicators for the months sensibly reduces the amount of overdispersion captured by the model.

A very large amount of clustering in the extended winter totals is suggested by Fig. 14. The dispersion first increases with the threshold, reaching values of above 1.0 for cyclones above the 60th quantile of vorticity, then decreases again. Uncertainty is here very large: at threshold $\bar{\xi}_{850} = 0$ ($\bar{\xi}_{850} = 0.6$), the 90 % confidence interval of ψ ranges from about 0 to 0.8 (respectively, 0.4 to over 1.4). A Poisson regression model is constructed as above, with the only difference that no seasonal indicators are used (that is, $k = 5$ in (5.2) and X_5 is a linear time trend). This model captures all of the features described above: in fact, the performance, as shown in Fig. 14, is better than for the monthly or 3-monthly counts. Indeed confidence intervals largely overlap and the point estimate of the dispersion in the Poisson model is close to the point estimate for the data. Also in this case, removal of the linear trend from the covariates does not significantly reduce the amount of modelled dispersion. The dispersion is much smaller (not shown), though still positive, if the extended winter transits are aggregated by calendar year, that is, if the Oct/Nov/Dec transits of a given year are aggregated with the Jan/Feb/Mar of the *same* year instead of the next. This aggregation procedure matches the way most reinsurance is purchased in Europe (although other parts of the world have significant renewals at other times).

Berlin (12.5E,52N)
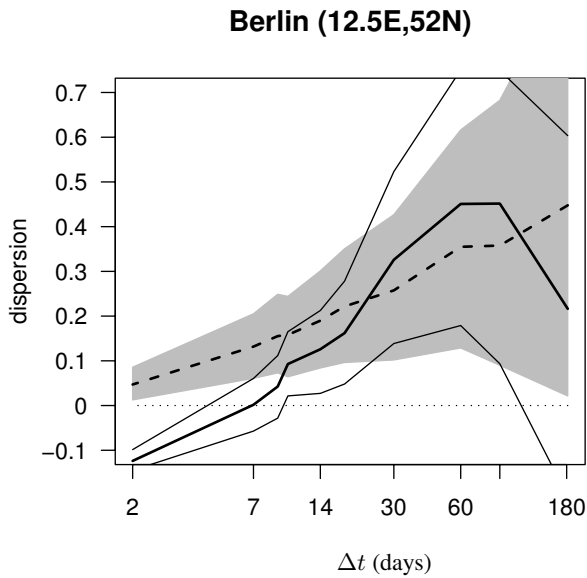
Figure 15: Same as Fig. 7 for a gridpoint near Berlin (solid lines). The dispersion simulated by a Poisson regression model fitted on the same data is plotted with dashed lines, 90 % bootstrap confidence intervals are rendered with grey shading.

Daily predictor (monthly counts)
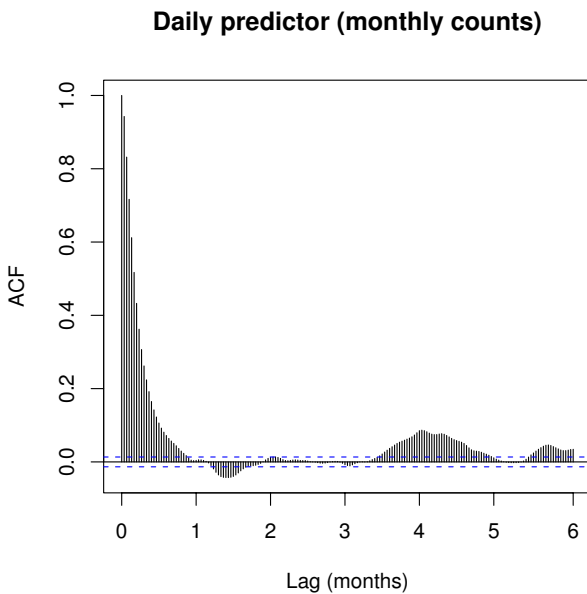
Figure 16: Autocorrelations of the time series of the daily Poisson predictor μ at Berlin with coefficients β_i estimated from a monthly model.

The large-scale flow also accounts for the dependence of the dispersion statistic on the aggregation period. Fig. 15 shows a plot, similar to Fig. 7, where the Poisson-simulated dispersion is also added (represented by grey shading). Notice that a different Poisson models is fitted for each value of Δt on the horizontal axis.

No seasonal indicator is included, as too many terms would be required for the shorter aggregation periods. These Poisson models reproduce the increasing trend of clustering with Δt as well as the magnitude of the uncertainty around the point estimate. Agreement is particularly good for aggregation periods between 14 and 90 days, whereas uncertainty increases for larger periods and is the dominant feature for 182 days (whole extended winter). Underdispersion appears for short aggregation periods (Δt below 7 days approximately). Here a limitation of the Poisson regression becomes obvious: Poisson models can only be equi- or over-dispersed. Hence, the dispersion simulated by the Poisson models is markedly larger than the observed dispersion for short aggregation periods.

The increase of clustering with aggregation period is potentially explained by small amounts of long-lead serial correlation in the teleconnection indices. The predictor μ in (5.2) is a time series μ_j, $j = 1, \dots, n_Y$, where n_Y is the length of the time series $Y = \{Y_j\}$ and $\log(\mu_j) = \beta_0 + \sum_{i=1}^{k} \beta_i X_i^j$. A monthly timescale Δt is selected and a Poisson model is constructed with seasonal indicators (see above), but without the time trend. The coefficients β_i are estimated from the time series of monthly counts at a gridpoint near Berlin. The time series μ_j is then generated using (5.2) with the daily teleconnection indices X_i and with the β_i from the monthly Poisson model. The autocorrelation of the daily time series μ_j drops to non-significant values within 15-20 days (Fig. 16). The same holds for the autocorrelation of the NAO index time series X_1^j (not shown). However, the autocorrelations of μ_j increase above significance from a lag of about 100 days. This feature is robust with respect to the aggregation period: values of Δt of 14 days and 1 year have also been examined, yielding consistent results. This is not an artifact of the exponentiation required to invert (5.2), since the same is obtained using the time series $\log(\mu_j)$. The long-lead serial correlation might possibly be a result of seasonality or intraseasonal persistence in the teleconnection indices. However, the monthly indicators included in the Poisson regression should account for the first effect, leaving the second as a potential mechanism explaining the increase of clustering with aggregation period.

In summary, the plots in Figs. 12 up to 15 illustrate the following features:

- overdispersion is present for all intensity thresholds: it initially increases with $\bar{\xi}_{850}$ and eventually decreases for large values of $\bar{\xi}_{850}$;

- increase of the dispersion with aggregation period (see the previous section) occurs coherently for a wide range of vorticity thresholds;

- uncertainty increases with aggregation period and is very large for the extended winter totals;

- the large-scale flow accounts for these features, since Poisson regression based on teleconnection indices captures the above characteristics.

These features are common among other locations: gridpoints near Paris, Copenhagen and London have been examined (figures not shown), yielding similar results. In fact, for these gridpoints the performance of the Poisson model is even better than that of the Berlin gridpoint presented above: in these cases, not only does the width of the confidence interval agree for the data and for the model-simulated dispersion, but also the point estimates are much closer, consistently for the monthly, 3-monthly and extended winter aggregation periods.

6   Conclusion

This study has investigated the dependence of clustering of wintertime extra-tropical cyclones on:

1. the vorticity (intensity) of the cyclones and

2. the length of the time period over which cyclone transits are counted.

3. the width of the latitudinal barrier used to define the cyclone transits.

Clustering is characterized by a dispersion statistic ψ defined as the deviation from unity of the ratio of variance to mean of the counts of eastward transits of cyclone tracks across meridian segments. Cyclone intensity is ranked according to the relative vorticity of the wind at 850 hPa. Intense cyclones are defined as those whose relative vorticity exceeds a fixed threshold $\bar{\xi}_{850}$, defined as a quantile of the vorticity distribution at each gridpoint.

Clustering is found to be largest for intense cyclones near the exit of the North Atlantic storm track. This region includes Scandinavia, UK, the Benelux countries, northern Germany and France. For a gridpoint near Berlin the dispersion statistic of the 3-monthly counts increases from 0.45 for all cyclones (threshold $\bar{\xi}_{850} = 0$) to 0.8 for cyclones with intensity in the upper 25 % of the vorticity distribution ($\bar{\xi}_{850} = 75$ %). The dispersion is positive for all considered threshold values. A 90 % confidence interval for ψ is bounded away from zero up to a threshold $\bar{\xi}_{850} = 90$ %. Uncertainties are large: a 90 % confidence interval for ψ is $(0.16, 0.76)$ for all cyclones and $(0.4, 1.17)$ for intensity threshold $\bar{\xi}_{850} = 85$ %.

The dispersion of the cyclone counts also increases with the length of the period Δt used to aggregate the transits. For $\Delta t = 4$ days the dispersion of the counts is -0.05 with 90 % confidence interval $(-0.09, 0)$: compare this with the values $\psi = 0.45$ and confidence interval $(0.16, 0.76)$ obtained for $\Delta t = 3$ months (see above). The dispersion scales linearly with the logarithm of Δt up to $\Delta t = 3$ months. For Δt equal to the whole extended winter, the dispersion drops to a

smaller (though still positive) value. However, uncertainty is very large: the 90 % confidence interval is here $(-0.15, 0.6)$. All these features are consistent across a number of locations in northern Europe, including gridpoints near London, Paris and Copenhagen.

Increased clustering with cyclone intensity and aggregation period has important implications for the accurate modelling of aggregate insurance losses. Our results suggest that windstorm clustering is of concern for companies with spatially extended insurance portfolios, such as (typical) reinsurance companies or large insurance groups. However, insurers with a more spatially localised portfolio might be affected by the accumulation of risk due to clustering of intense cyclones even if these do not qualify as catastrophic windstorms, also in view of the capital requirements discussed in the Introduction.

The time-varying effect of large-scale atmospheric flow largely accounts for the increases in dispersion discussed above. Four of the main teleconnection indices affecting atmospheric variability in the Northern Hemisphere are used as covariates in nonlinear Poisson regression models. The teleconnection indices used here are the North Atlantic Oscillation, the East Atlantic Pattern, the Scandinavian pattern, and the East Atlantic/West Russia pattern. The Poisson models reproduce both the increases and the sampling uncertainties in the dispersion when either intensity threshold or aggregation period is varied. Increased dispersion for more intense cyclones is explained by an increased effect of the indices on the cyclone transit rates. Increased dispersion for longer aggregation periods is related to small amounts of serial correlation which are found in the indices and in the transit rate predictor at long lags (> 100 days).

A limitation of the present approach is that separate Poisson models must be fitted for different values of the vorticity threshold and of the aggregation period: this means that some information is being discarded. Future research will aim at constructing models, based on marked non-stationary Poisson processes in the time axis (COX and ISHAM, 1980), which can simultaneously account for the complex features described above.

A   Poisson regression

Cyclone count data are often modelled by Poisson regression (ELSNER and SCHMERTMANN, 1993; MC-DONNELL and HOLBROOK, 2004), see CAMERON and TRIVEDI (1998); MCCULLAGH and NELDER (1989) for general introductions. A time series Y of count data is

assumed to be a sample of a Poisson distribution whose mean is conditional on the value of k time-varying factors $X_1, X_2, \ldots, X_k$. For cyclone counts, equation (5.2) means that the rate of cyclone arrivals depends on the time-varying effect of the explanatory factors X_i. Equation (5.1) prescribes the variability of the cyclone counts around the conditional mean μ: this is aleatory (random, stochastic) variability, with the shape of a Poisson distribution.

The dispersion captured by the Poisson model (represented with grey shading in Fig. 12) is computed by parametric bootstrap: a value of the threshold $\bar{\xi}_{850}$ is fixed and a Poisson model as in (5.1)- (5.2) is fitted to the corresponding time series of aggregate counts. Seasonal factors and a linear time trend are added to the covariates since overdispersion might be accounted for by non-stationary effects (rather than by the large-scale flow). The fitted value of μ is a sequence $\{\mu_j, j = 1, \ldots, n_Y\}$ with one conditional mean for each observation y_j in $Y = \{y_j, j = 1, \ldots, n_Y\}$. For each j, a sample of length one is drawn from a Poisson distribution with mean $\{\mu_j\}$: this gives a sequence of numbers which is a realisation $\bar{Y}$ of the variable (5.1). Mean and variance are computed for $\bar{Y}$, from which an estimate $\bar{\psi}$ of the dispersion statistic is obtained. This process is iterated, producing a sample of values of $\bar{\psi}$. The mean of this sample is plotted with a dashed line in Fig. 12 and a 90 % confidence interval, determined by the 5 % and 95 % quantiles of the same sample, is rendered with grey shading. The same approach is used for Fig. 15: in this case, a different Poisson model is fitted to the count time series obtained for each Δt.

Significance of the dispersion statistic is determined by LM tests for overdispersion against the Katz system (CAMERON and TRIVEDI, 1998, Sec. 5.4.1), where the test statistic is:

$$T_{LM} = \frac{1}{2} \sum_{j=1}^{n_Y} \left[(y_j - \mu_j)2 - y_j \right] \Big/ \sqrt{\frac{1}{2} \sum_{j=1}^{n_Y} \mu_j 2}\,.$$

References

BARNSTON, A.G., R.E. LIVEZEY, 1987: Classification, seasonality and persistence of low-frequency atmospheric circulation patterns. – Mon. Wea. Rev. **115**(6), 1083–1126.

BRESCH, D.N., M. BISPING, G. LEMCKE, 2000: Storm over europe: an underestimated risk. Technical report, Swiss Reinsurance Group, Mythenquai 50/60, P.O. Box CH-8022, Zurich.

CAMERON, C.A., P.K. TRIVEDI, 1998: Regression Analysis of Count Data (Econometric Society Monographs) – Cambridge University Press.

COX, D.R., V. ISHAM, 1980: Point Processes CRC Monographs on Statistics & Applied Probability. – Chapman & Hall/CRC.

DAVISON, A.C., D.V. HINKLEY, 1997: Bootstrap Methods and Their Application (Cambridge Series in Statistical and Probabilistic Mathematics , No 1) – Cambridge University Press.

ELSNER, J.B., C.P. SCHMERTMANN, 1993: Improving extended-range seasonal predictions of intense atlantic hurricane activity. – Wea. Forecast. **8**(3), 345–351.

HODGES, K.I., 1994: A general method for tracking analysis and its application to meteorological data. – Mon. Wea. Rev. **122**(11), 2573–2586.

—, 1995: Feature tracking on the unit sphere. – Mon. Wea. Rev. **123**(12), 3458–3465.

—, 1996: Spherical nonparametric estimators applied to the ugamp model integration for amip. – Mon. Wea. Rev. **124**(12), 2914–2932.

—, 1999: Adaptive constraints for feature tracking. – Mon. Wea. Rev. **127**(6), 1362–1373.

KALNAY, E., M. KANAMITSU, R. KISTLER, W. COLLINS, D. DEAVEN, L. GANDIN, M. IREDELL, S. SAHA, G. WHITE, J. WOOLLEN, Y. ZHU, A. LEETMAA, R. REYNOLDS, M. CHELLIAH, W. EBISUZAKI, W. HIGGINS, J. JANOWIAK, K.C. MO, C. ROPELEWSKI, J. WANG, R. JENNE, D. JOSEPH, 1996: The ncep/ncar 40-year reanalysis project. – Bull. Amer. Meteor. Soc. **77**(3), 437–471.

KVAMSTØ, N.G., Y. SONG, I.A. SEIERSTAD, A. SORTEBERG, D. B. STEPHENSON, 2008: Clustering of cyclones in the ARPEGE general circulation model. – Tellus A **60**(3), 547–556.

MAILIER, P.J., 2007: Serial Clustering of Extratropical Cyclones – PhD in Meteorology, University of Reading.

MAILIER, P.J., D.B. STEPHENSON, C.A.T. FERRO, K.I. HODGES, 2006: Serial clustering of extratropical cyclones. – Mon. Wea. Rev. **134**(8), 2224–2240.

MCCULLAGH, P., J. NELDER, 1989: Generalized Linear Models Monographs on Statistics & Applied Probability. – Chapman & Hall/CRC.

MCDONNELL, K.A., N.J. HOLBROOK, 2004: A poisson regression model of tropical cyclogenesis for the australian-southwest pacific ocean region. – Wea. Forecast. **19**(2), 440–455.

RUELLE, D., 1990: The Claude Bernard Lecture, 1989. Deterministic chaos: the science and the fiction. – Proc. Roy. Soc. London Ser. A **427**(1873), 241–248.

SMITS, A., A.M.G. KLEIN TANK, G.P. KÖNNEN, 2005: Trends in storminess over the netherlands, 1962-2002. – Int. J. Climatol. **25**(10), 1331–1344.

STERL, A., 2004: On the (in)homogeneity of reanalysis products. – J. Climate **17**(19), 3866–3873.

VENABLES, W.N., B.D. RIPLEY, 1994: Modern applied statistics with S-Plus Statistics and Computing. – Springer-Verlag, New York, xiv+462.

WILLIS ANALYTICS, 2007: Windstorm Kyrill, 18 January 2007. – Technical report, Willis Re Inc., The Willis Building, 51 Lime Street, London EC3M 7DQ.